Construction and Building Materials 94 (2015) 181–188

Contents lists available at ScienceDirect

Construction and Building Materials

journal homepage: www.elsevier.com/locate/conbuildmat

Influence of nano-silica addition in the durability of UHPC

Ehsan Ghafari [a,*], Mahdi Arezoumandi [b], Hugo Costa [c], Eduardo Júlio [a]

[a] ICIST, IST-University of Lisbon, Portugal
[b] Missouri Science and Technology University, Rolla, MO, USA
[c] ICIST, ISEC-Polytechnic Institute of Coimbra, Portugal

HIGHLIGHTS

- The time to cracking in HPC is less than half the time in UHPC.
- The addition of nS to UHPC effectively reduces the corrosion rate of steel bars.
- A new corrosion test procedure has been used to assess the corrosion rate.
- The corrosion test procedure was found to be useful to assess the corrosion rate.

ARTICLE INFO

Article history:
Received 24 December 2014
Received in revised form 20 April 2015
Accepted 6 July 2015

Keywords:
UHPC
Nano-silica addition
Corrosion resistance
Tafel test
LPR

ABSTRACT

This study aims at studying the effect of nano-silica (nS) addition to ultra-high performance concrete (UHPC) on the corrosion resistance of steel bars embedded in the latter. In order to conduct a comparative study, a high performance concrete (HPC) and an UHPC without nS were also considered in the experimental program. An accelerated corrosion test along with multi-steps potentiodynamic polarization technique, including Tafel plot and linear polarization resistance (LPR), was used to determine the corrosion rate of the samples tested. The accelerated corrosion tests showed that the time to cracking in HPC is less than half the time in UHPC. It was found that nS addition to UHPC effectively reduces the corrosion rate of steel bars embedded in the latter.

1. Introduction

Nowadays, sustainability should be the major priority of the construction sector. Regarding this matter, being concrete the world's most widely used construction material, it requires special attention. Sustainability in concrete structures involves design for long-term durability, having simultaneously a minimal impact on the environment considering the structure's life-cycle [1]. Therefore, long-term durability is a prominent feature of sustainability of concrete structures, since extending their service life, through enhanced durability, has considerable advantages in terms of optimizing resources and of reducing maintenance operations [2]. Considering that reinforced concrete structures experience deterioration during their service life, caused by physical and chemical attacks, the definition of durable concrete structure corresponds to that in which degradation occurs at reduced rate and thus it does not affect its structural performance within its life-time [3].

The most important deterioration mechanism registered in concrete structures is the corrosion of reinforcing bars, mainly due to carbonation or chloride ingress in concrete. It is estimated that circa 60% of Europe's annual budget of the construction sector is spent on the rehabilitation of existing structures, corresponding to US$ 5 billion, only in Western Europe [4]. The annual direct cost of corrosion for highway bridges in the U.S. is estimated at US$ 8.3 billion, referring to the budget to replace or maintain structurally deficient bridges [5]. Therefore, the development of innovative durable materials and methods aiming at extending the life-time of both existing and new structures, without or with reduced maintenance costs, is a key-issue. Regarding concrete structures, durability depends mainly on the cover. In this scope, the ideal scenario consists in designing a composite concrete-to-concrete cross-section, having a high durability concrete cover and a current concrete bulk.

The superior mechanical properties and higher durability of ultra-high performance concrete (UHPC) has been widely reported

* Corresponding author.
E-mail addresses: ghafari@dec.uc.pt (E. Ghafari), ma526@mst.edu (M. Arezoumandi), hcosta@isec.pt (H. Costa), eduardo.julio@tecnico.ulisboa.pt (E. Júlio).

http://dx.doi.org/10.1016/j.conbuildmat.2015.07.009
0950-0618/

[6–8]. This makes it an ideal material for several structural applications, particularly rehabilitation of concrete structures [9–13], and an ideal material for the high-durability cover previously referred to. In previous studies [14,15], the authors proved that the addition of nS particles leads to a reduction of capillary pores and to a refinement of the pore structure of UHPC. It has also been proved that the inclusion of nS improves the durability of concrete [16,17]. He et al. [18] concluded that an addition of nS and nano-clay significantly improves the chloride penetration resistance as well as the general ionic permeability of Portland cement based mortars. It is also reported that the addition of nS, especially at higher replacement levels, enhances the chloride and electrical resistance of concrete [19–21].

The study herein reported is part of a wider research project aimed at developing an ultra high durability concrete (UHDC) cover that can be applied in new constructions, as well as in the rehabilitation of existing structures, with the goal of considerably enhancing their life-time. In this scope, it was decided to conduct the experimental research described ahead, with the specific goal of assessing the influence of nano-silica addition in the durability of UHPC, namely by evaluating the chloride induced corrosion resistance using acceleration corrosion tests along with multi-steps potentiodynamic polarization technique. In order to compare results, an UHPC without nS and a high performance concrete (HPC) were also considered in the experimental program described ahead.

2. Experimental program

2.1. Materials properties and mixture proportions

Portland cement type I 52.5R, an addition of silica fume (SF) presenting a specific area of 18.41 m^2/g, and an addition of nS with an average particle size of 15 nm were adopted in the present study. In Table 1 the relevant physical and chemical properties of cement and silica fume are shown and, in Table 2, the properties of nS are summarized. SEM micrographs of nS particles are also presented in Fig. 1, where it can be seen that these exhibit a spherical shape. In UHPC mixtures, siliceous sand aggregate, with 0.6 mm of maximum aggregate size, was used. Medium sand, with 5 mm maximum size, and coarse limestone aggregate, with 16 mm of maximum aggregate size, were also used in HPC mixture. A polycarboxylic acid based superplasticizer (SP), with solids content between 28.5 and 31.5 wt.% and density of 1.087 g/cm^3, was adopted as admixture.

The mixing procedure involved several steps. First, in order to prevent agglomeration and also to promote a uniform distribution of very fine particles, all powders and siliceous sand were dry mixed during 5 min at low speed. The addition of dry nS was not possible, due to its very low density, which would cause particles to disperse in the air. Therefore, nS was first dissolved in water already containing the superplasticizer, and then gradually added to the mixture. After 5 min, the mixture became fluid [22,23].

Three different sets of mixtures were considered for this test (Table 3), consisting of UHPC containing nS, UHPC without nS, and high performance concrete (HPC). The mixture proportion of UHPC was obtained based on extensive series of both numerical and experimental studies conducted by the authors [24–27]. Also according to previous studies by the authors [14,15], a 3 wt.% replacement of cement by nS in cement paste was assumed as optimum, i.e. as the value leading to the best material performance.

Table 1
Chemical composition and physical properties of cement and silica fume.

Chemical analysis (%)	Cement	Silica fume
SiO_2	20.9	93.6
Al_2O_3	4.60	1.3
Fe_2O_3	3.15	0.90
CaO	62.0	0.4
MgO	2.00	1
SO_2	3.60	0.4
K_2O	<1	1.52
Na_2O	<1	<1
Specific gravity	3.14	2.17

2.2. Test procedure

2.2.1. Accelerated corrosion test

An accelerated corrosion test was used to determine the corrosion resistance of concrete specimens [28–30]. In this context, concrete cylinders, embedding a 16 mm diameter rebar were immersed in a 5% NaCl solution by weight of water. Two specimens were produced for each concrete mixture. A solution tank was prepared and filled up to mid-height with all concrete specimens, which were tested at the age of 28 days. The corrosion procedure started by applying an anodic potential of 30 V across the specimens, using the steel rod as positive electrode and the steel mesh as negative electrode. The variation of current with time and the time up to failure of the reinforced concrete specimens were recorded for each specimen using a data logger. Cracking of specimens was easily identified since the current increased abruptly [31]. A schematic picture of the experimental setup for the accelerated corrosion test is shown in Fig. 2.

2.2.2. Potentiodynamic polarization tests

Potentiodynamic polarization tests were performed using a CompactStat running with IviumSoft 2.124. The measurements were carried out using a three-electrode system in the same set-up of accelerated corrosion test above described. The corrosion cell consisted of a working electrode (steel rebars), a counter electrode (steel plate) and a silver/silver chloride reference electrode Ag/AgCl (3 M KCl). Fig. 3 shows the setup for potentiodynamic polarization tests. The main objective of potentiodynamic tests was to measure the corrosion current density and corrosion rate of steel bars embedded in the concrete specimens. The corrosion current is the rate with which the anodic or cathodic reactions are occurring on the working electrode. The current is expressed in terms of the current per unit area of the working electrode, or the corrosion current density (I_{corr}). However, the corrosion current density cannot be directly measured in the absence of any applied potential, since the production of electrical charges at the anode is exactly equal to its consumption at the cathode to maintain equilibrium of the charges with a zero net current [32]. Hence, several analysis techniques such as polarization resistance, Tafel, and cyclic polarization have been used to measure the corrosion current density. The difference was the range to which the specimen was polarized and how the data from the test was analyzed [33]. In this study both Tafel plot and linear polarization techniques were used to determine the I_{corr} and corrosion rate of steel bars. The LPR test was performed first to minimize the effect of potential perturbation of the reinforcing steel between the two experiments [32].

2.2.2.1. Tafel analysis. Tafel technique involves applying a potential scan to the specimen starting from E_{corr} and extending to a few hundred millivolts (about 250 mV) either in the cathodic or in the anodic direction. In this study the Tafel plots were recorded between −1.00 and +1.00 V at a scan rate of 1 mV/s.

The Tafel equations estimate a straight line for the variation of the logarithm of the current density with potential. The currents are shown in logarithmic plots known as Tafel plots. This type of analysis is referred to as Tafel slope analysis [34]. A schematic picture of Tafel plot is shown in Fig. 4. It presents a linear part, and the slopes known as Tafel constants, namely the anodic Tafel constant and the cathodic Tafel constant. Although these two constants are not required for corrosion rate calculations in Tafel technique [35], they can be used for the calculation of corrosion rate using polarization resistance technique as described in the following section.

In order to calculate the corrosion rate, first the corrosion current density (I_{corr}) needs to be determined. The latter can be calculated using Tafel slope analysis. As shown in Fig. 4, the intersection of the projection of the linear part of the plot with E_{corr} gives I_{corr}. The relation between current density and potential of anodic and cathodic electrode reactions under charge transfer control is given by the Butler–Volmer equation (Eq. (1)) [36]:

$$I(E) = I_{corr} \cdot \left[e^{2.303 \frac{E - E_{corr}}{\beta_a}} - e^{2.303 \frac{E - E_{corr}}{\beta_c}} \right] \quad (1)$$

where $I(E)$ – net current differential between the anodic and cathodic reactions; E – applied potential; I_{corr} – the corrosion current; E_{corr} – potential, where $I(E) = 0$; β_a and β_c – respective rates of the anodic and cathodic current change versus potential.

Once I_{corr} is determined, the following equation (Eq. (2)), derived from Faraday's law, can be used to calculate the corrosion rate [37,38]:

$$CR\,(\mu m/y) = \frac{3.27 \times I_{corr} \times \text{E.W.}}{d} \quad (2)$$

where I_{corr} is calculated form Eq. (1), and E.W. is the equivalent weight of steel in g and d is the density of the reinforcing bar in g/cm^3.

2.2.2.2. Linear polarization resistance technique. The linear polarization resistance (LPR) technique has been widely used in determining corrosion rates of steel rebars in concrete [39]. In this technique, a potential scan is applied to the specimen relatively to its Open Circuit (OC) potential in a range much smaller than that used in

Table 2
Properties of nS.

Formula	Specific surface area (m^2/g)	Purity	Crystal phase	Diameter (nm)	Density (g/cm^3)	Morphology
SiO_2(nS)	160 ± 20	>99.9 (%)	Amorphous	15 ± 5	<0.15	Spherical

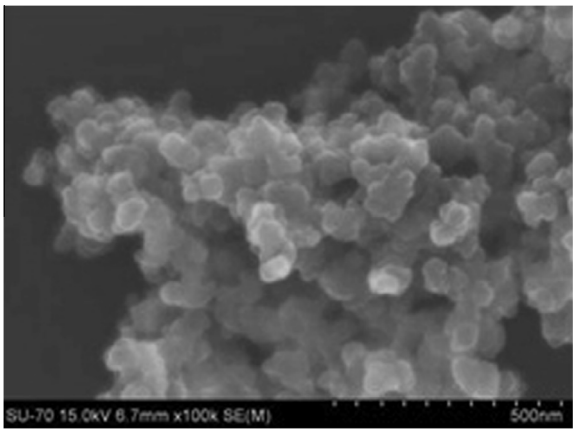

Fig. 1. SEM micrograph of nS particles.

the Tafel plot technique. In this study the specimens were polarized from $E_{oc} - 20$ mV to $E_{oc} + 20$ mV. The polarization resistance is defined as the ratio between the potential variation and the current variation.

The polarization resistance (R_p) can be related to the corrosion current density (I_{corr}), using the Stern–Geary equation (Eq. (3)) [40]:

$$I_{corr} = \frac{B}{R_p} \tag{3}$$

where B is a constant based on both anodic and cathodic Tafel constants (B_a and B_c) [41], and it can be calculated using Eq. (4).

$$B = \frac{B_a \times B_c}{2.303(B_a + B_c)} \tag{4}$$

3. Results and discussion

3.1. Accelerated corrosion test

An accelerated corrosion test was performed to determine the behavior of steel rebars embedded in concrete specimens. The current required to keep constant the voltage of the corrosion cell was recorded through time. In Fig. 5 the mean variation of corrosion current with time is plotted for each mixture. It can be observed that the measured value was constant during a certain period of time, for all specimens, beyond which an abrupt increase occurs. This significant current change corresponds to the instant when concrete specimens cracked due to rebar corrosion [30,31], as illustrated in Fig. 6.

The corrosion time of the specimens were marked in Fig. 6 as well as been presented in Table 4. It can be seen that the time needed to crack HPC specimens was 3600 min, i.e. less than half the time obtained with UHPC specimens, the latter varying in the range of 7000–8800 min. In addition, it can be seen that the time to cracking was effectively increased by adding nS. Although

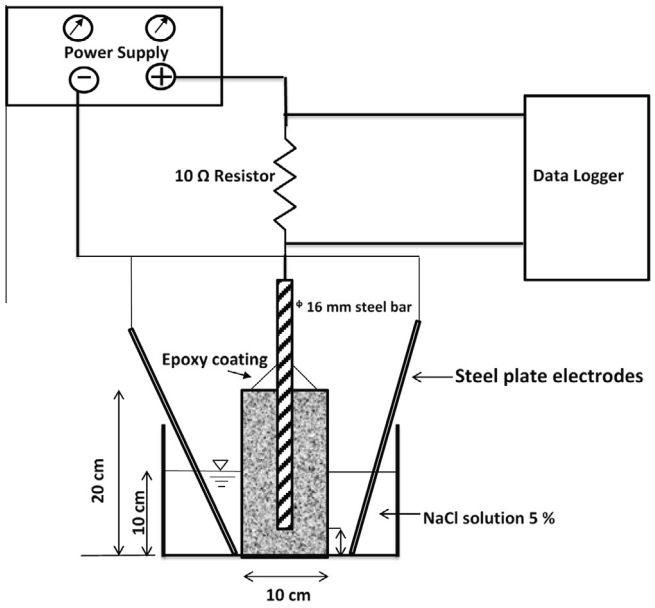

Fig. 2. Accelerated corrosion measurements set-up.

the increase in time needed to reach cracking can be considered as an increase of corrosion resistance of steel rebar in concrete specimens, it does not represent the real corrosion resistance of the latter for the reasons presented next. In fact, this test identifies the instant cracking of the specimens occurs, and not the instant of corrosion initiation. Furthermore, with this test the corrosion rate is not determined, being this the main parameter in prediction models of service life of RC structures [42]. After performing some trial accelerated corrosion tests, the average time needed to crack specimens was determined. Afterwards, this period was divided into three main zones (Fig. 5) in which the corrosion rate of the steel bars was measured by potentiostatic polarization tests at three different steps. As shown, the time of corrosion test at each step was defined according to the time to crack analysis. The time step for each of the three mixtures is presented in Table 4. However UHPC and UHPC-nS specimens were tested at the same time at each step of polarization test.

3.2. Tafel analysis results

Tafel analysis was conducted to determine the corrosion rate of the specimens. The E_{corr} and R_p were calculated from Tafel plots at the zero current intersection point. Table 5 summarizes the obtained results of Tafel analysis.

Figs. 7–9 show the Tafel curves recorded for three samples of HPC, UHPC and UHPC-nS at three steps of Tafel polarization test.

Table 3
Composition of UHPC mixture (by weight, kg/m^3).

Sample	Cement	Coarse aggregate	Sand (2–5 mm)	Sand (0–0.6 mm)	SF	nS	Water	SP
HPC	475	971	386	272	119	–	161	12
UHPC	941.5	–	–	873	255	–	189	31
UHPC-nS	921.5	–	–	873	255	28.5	189	31

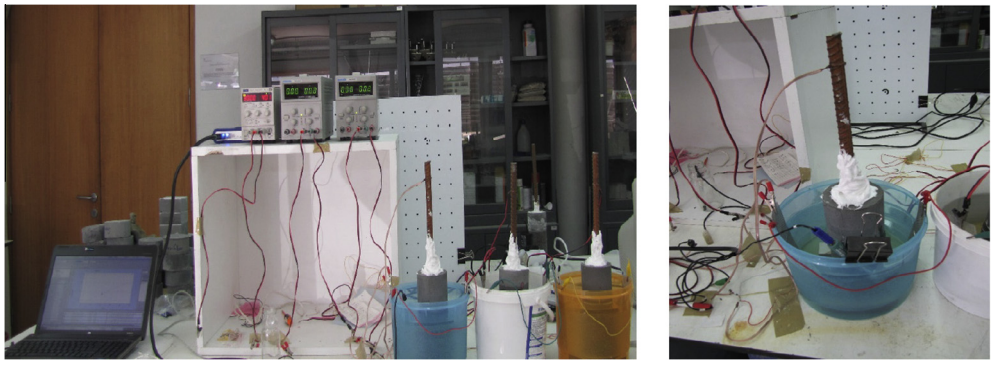

Fig. 3. Corrosion rate measurements set-up.

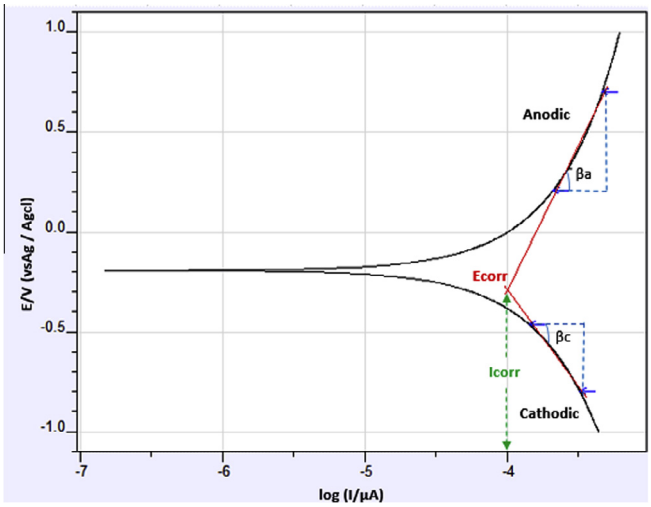

Fig. 4. Idealized Tafel plot.

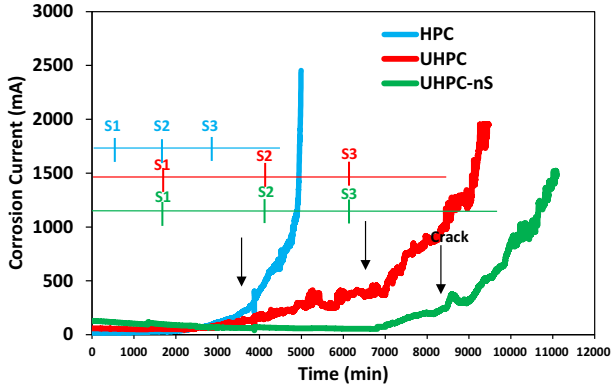

Fig. 5. Typical curve of corrosion current versus time at the test age of 28 days for HPC, UHPC and UHPC-nS.

The measured values of E_{corr} at the first step of the polarization test were: +0.046, −0.408, and −0.116 V, for HPC, UHPC and UHPC-nS, respectively. The corresponding values of I_{corr} were: 307, 222 and 101 μA. The higher corrosion density in HPC indicates a lower polarization resistance (299 Ω), which in turn results in a higher corrosion rate.

The evolution of corrosion potential and current corrosion density during the three steps of Tafel polarization test are shown in Figs. 10 and 11, respectively. It can be seen that, at the second step of polarization test, the corrosion potential of UHPC increased to −0.132 V, whereas the corrosion current decreased to 67 μA. This effect is due to the development of a protective oxide layer on the surface of the steel rebars. The decrease of I_{corr} indicates that the steel rebar remained passivated even when more chloride ion reached the surface. According to Table 5, the polarization resistance of UHPC increased up to 3619 Ω, which is 4.42 times higher than the value obtained in the first step of polarization Tafel test.

A similar behavior was observed for HPC, in which the formation and growth of a passive film on the surface of the steel rebar led to a significant increase in the polarization resistance. In spite of a dramatic decrease of the corrosion current density, HPC showed a continuous time-dependent decrease of the corrosion potential along the second step of polarization test (Fig. 10). Results showed that R_p increased to 2494 Ω, which is almost 8.3 times higher than the value obtained in the first step of the potential test.

Fig. 10 also shows that the corrosion potential of UHPC-nS slightly increased at the second step of the polarization test. From Fig. 11, it can be seen that the corrosion current kept an approximately constant value, while the resistance slightly increased up to 2844 Ω, which is only 1.1 higher than the value in the first step of polarization test. This negligible variation in corrosion density and polarization results implied that the chloride ions have not reached the surface of steel rebars. A delay in the formation of the oxide layer for these specimens may explain their higher corrosion resistance.

By increasing the time of the accelerated corrosion, more chloride ions can diffuse through the capillary pores of concrete toward the steel rebar, leading to an increase in the corrosion current density. Only after the chloride ions reached a certain concentration, the active corrosion could be initiated.

Fig. 10 shows a significant decrease in the value of the corrosion potential at the third step of polarization test for all three specimens. For HPC, the corrosion potential dropped suddenly 0.395 V, reaching circa −0.690 V, and the corrosion current density increased significantly from 109 μA (passive state) to 790 μA (active corrosion). Results show that the polarization resistance of HPC dropped almost 10 orders of magnitude, namely from 2491 to 261 Ω.

The corrosion potential of UHPC also dropped significantly down to −0.475 V, whereas the corrosion current density increased up to 375 μA. The polarization resistance of UHPC decreased sharply down to 401 Ω, which is almost 8 times lower than the value obtained in the second step of polarization test.

Similarly to HPC and UHPC, a significant decrease in the potential current of UHPC-nS was observed. Results show that the E_{corr} of UHPC-nS dropped down by a significant amount of −0.511 V, reaching −0.580 V. However, as shown in Fig. 6, a slight increase was observed in the corrosion current density. The polarization

Fig. 6. Typical corrosion specimens after the accelerated corrosion test.

Table 4
The corrosion time of specimens and the three steps of potentiodynamic polarization test.

Sample	Time (min)			
	Crack	Step 1	Step 2	Step 3
HPC	3600	0–500	500–1750	1750–3000
UHPC	7000	0–1750	17,501–4200	4200–6500
UHPC-nano	8800	0–1750	1750–4200	4200–6500

resistance dropped only circa 2.6 orders of magnitude, from 2844 to 1066 Ω. These results proved that the nS addition effectively improves the corrosion resistance of rebars embedded in the UHPC sample.

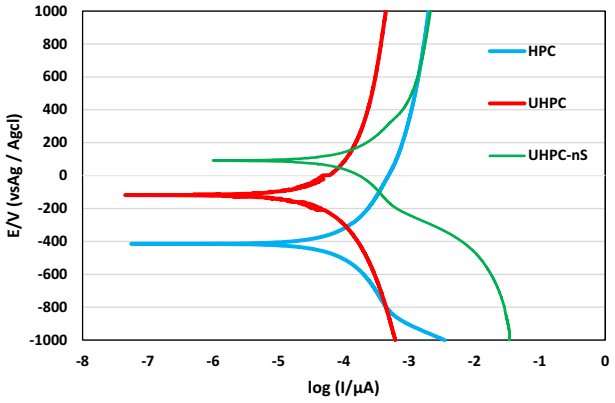

Fig. 7. Tafel curves of HPC, UHPC and UHPC-nS at the first step of polarization test.

3.3. Linear polarization resistance results

Figs. 12–14 shows the linear polarization resistance (LPR) curves recorded for three mixtures (HPC, UHPC and UHPC-nS) at three steps of LPR test. In order to calculate the corrosion current density, B was calculated from the anodic (β_a) and cathodic (β_c) Tafel slopes, which were determined by Tafel analysis. All the polarization test results are presented in Table 5. The variation in polarization resistance of HPC, UHPC and UHPC-nS during all steps of LPR test is shown in Fig. 15. One can see that, at the first step of the polarization test, the UHPC-nS exhibited the highest R_p value, while HPC showed the lowest amount of R_p. At the second step of the LPR test, a significant increase in the polarization resistance can be observed for all specimens. This can be related to the formation of the passive layer. In fact, the variation in the polarization resistance of UHPC-nS between two steps was lower than in other mixtures, which implies the better corrosion resistance performance of UHPC with nS addition. The results of LPR test at the third step indicate that the polarization resistance of HPC dropped significantly down to 252 Ω, which is almost 7 times lower than the value obtained in the second step of the polarization test. Also the R_p of UHPC and UHPC-nS dropped down by 5.8 and 2.1 order of magnitude, respectively. In general, the results analysis of LPR tests indicate a similar corrosion behavior for all mixtures as

Table 5
Tafel test and LPR results for HPC, UHPC and UHPC-nS.

Sample	Time	Tafel analysis					LPR	
		E_{corr} (V)	I_{corr} (μA)	R_p (Ω)	B_a (V/dec)	B_c (V/dec)	I_{corr} (μA)	R_p (Ω)
HPC	First step	0.046	307	299	1.17	0.40	314	412
	Second step	−0.195	109	2494	1.45	0.96	155	1615
	Third step	−0.690	790	261	1.73	0.66	824	252
UHPC	First step	−0.408	222	818	1.50	0.35	131	940
	Second step	−0.132	67	3619	1.33	0.96	92	2643
	Third step	−0.475	375	401	1.73	0.67	465	451
UHPC-nS	First step	−0.116	101	1580	1.63	0.94	182	1420
	Second step	−0.044	94	2844	1.49	1.05	126	2121
	Third step	−0.377	219	1066	1.86	0.75	223	1039

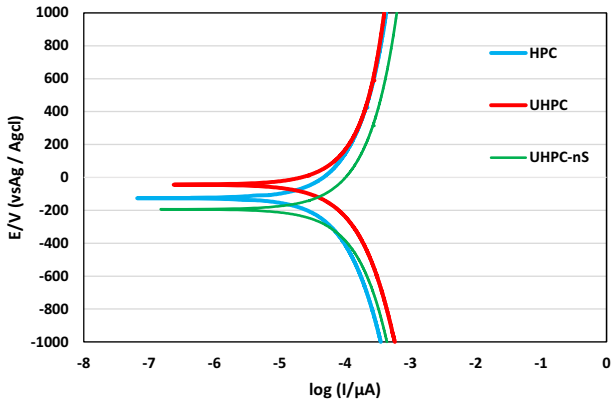

Fig. 8. Tafel curves of HPC, UHPC and UHPC-nS at the second step of polarization test.

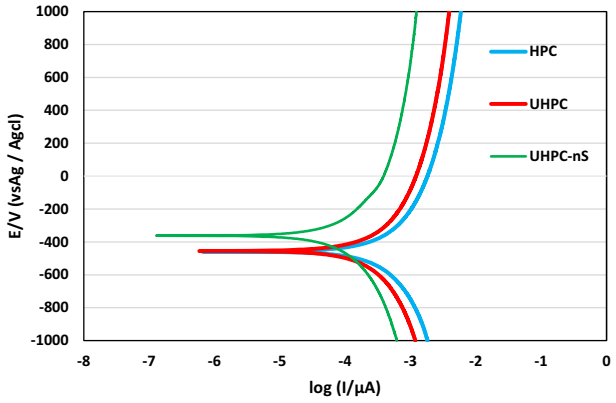

Fig. 9. Tafel curves of HPC, UHPC and UHPC-nS at the third step of polarization test.

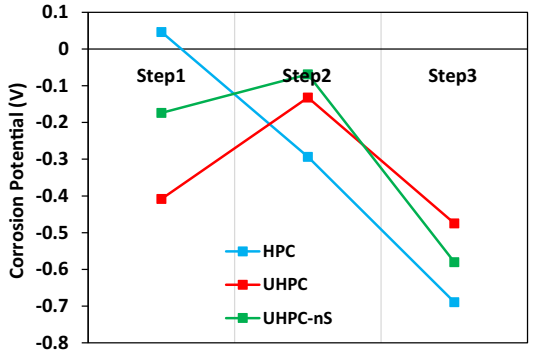

Fig. 10. Variation of the corrosion potential of HPC, UHPC and UHPC-nS during three steps of polarization test.

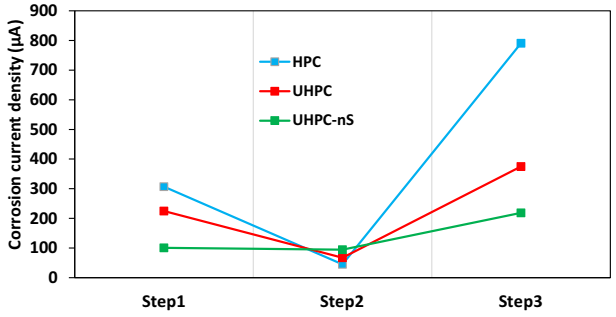

Fig. 11. Variation of the corrosion current density of HPC, UHPC and UHPC-nS during three steps of polarization test.

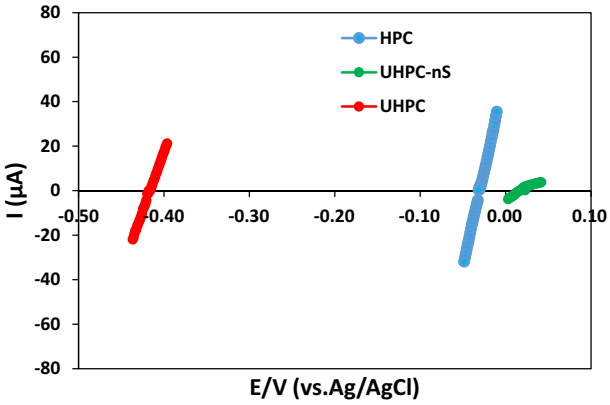

Fig. 12. LPR test curves of HPC, UHPC and UHPC-nS at the first step of polarization test.

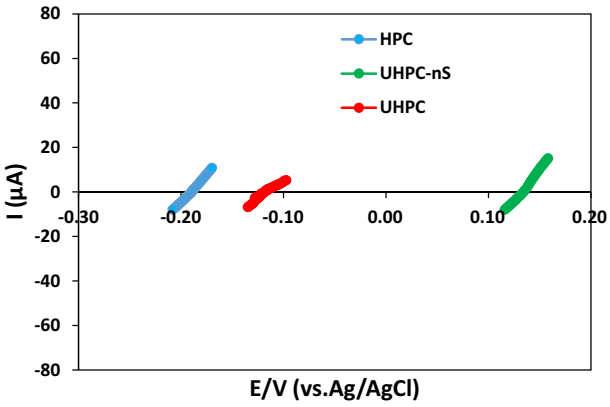

Fig. 13. LPR test curves of HPC, UHPC and UHPC-nS at the second step of polarization test.

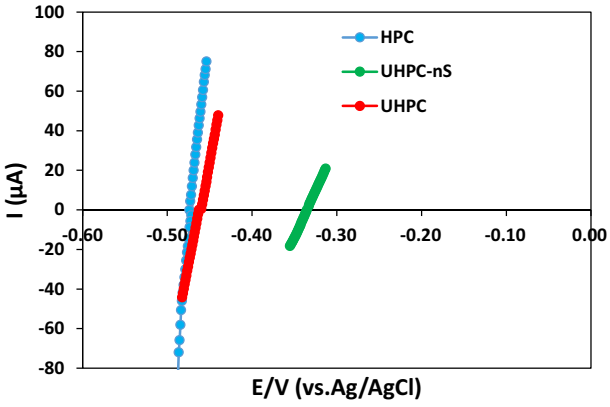

Fig. 14. LPR test curves of HPC, UHPC and UHPC-nS at the third step of polarization test.

compared with Tafel analysis results. As shown, the higher polarization resistance of UHPC-nS along with lower corrosion current indicate the enhancement of corrosion resistance of this mixture.

3.4. Determination of corrosion rate

The corrosion rates of the mixtures were calculated using both the Tafel technique and the LPR test. Fig. 16 shows the corrosion

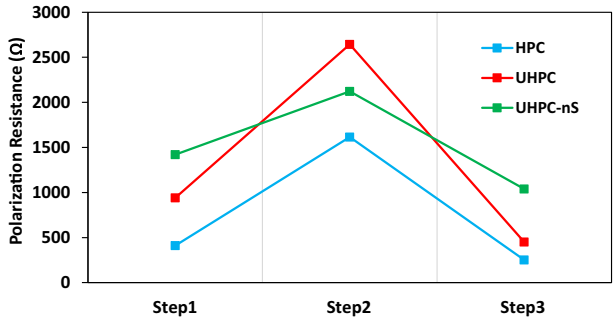

Fig. 15. The variation in polarization resistance of HPC, UHPC and UHPC-nS during the all three steps of LPR test.

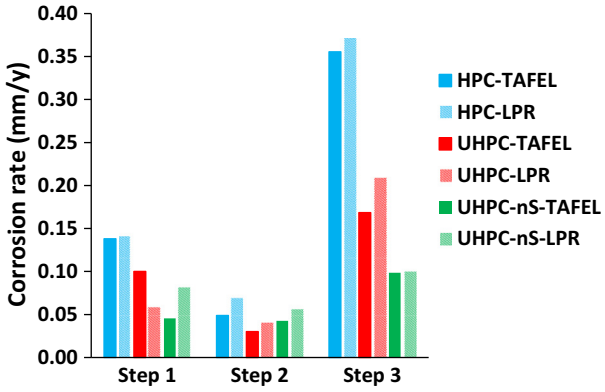

Fig. 16. Corrosion rate of steel bars for HPC, UHPC and UHPC-nS obtained by Tafel and LPR techniques at three different steps of polarization test.

rate of steel rebars for HPC, UHPC and UHPC-nS, obtained by Tafel and LPR techniques at three different steps of the polarization test. The corrosion rate decreased in the second step, due to the formation of a passive film. However, as more chloride ions reached the surface of steel rebars, the corrosion rate significantly increased.

The results obtained by Tafel analysis indicate that the corrosion rate of HPC increased from 0.05 up to 0.36 mm/y. Also the corrosion rate of UHPC increased from 0.03 to 0.17 mm/y. However UHPC-nS showed the lowest increment (up to 0.1 mm/y) in corrosion rate, only 2.5 times the rate at passive corrosion.

In Fig. 16, HPC shows the highest corrosion current density at the first and at the third steps of polarization tests, whereas UHPC-nS has the lowest corrosion rate. The active corrosion rate of HPC is 2.1 higher than the corresponding value of UHPC and 3.6 times higher that of UHPC-nS. It has to be noted that UHPC and HPC showed almost the same corrosion potential at the third step of Tafel polarization test. However, the corrosion rate of UHPC is two times lower than that of HPC. Thus, the corrosion potential itself cannot be considered as a reliable indicator of the real corrosion behavior of steel rebars embedded in concrete specimens.

The inclusion of nS was found to be effective in reducing the corrosion rate of steel rebars embedded in UHPC, since the active corrosion rate in UHPC-nS was much lower, by 41%, than that in UHPC. The corrosion rate obtained by LPR test also corroborates the results of Tafel analysis. However, the corrosion rates achieved using the LPR technique are higher than those obtained using the Tafel plot technique. A similar result has been reported in other studies [32].

The difference in corrosion rates is different enough to assert that an nS addition to UHPC reduces the corrosion rate of steel rebars, since it leads to a more refined pore structure. In fact, most aspects of concrete durability are directly related with its porous structure, since capillary pores are responsible for fluids' migration in the concrete matrix. Therefore, as the value of capillary pores decreases, the resistance to aggressive environments improves significantly.

The accelerated corrosion tests, combined with the multi-steps corrosion potential tests, were efficient in studying the corrosion behavior of steel rebars in concrete specimens. The obtained corrosion rate at first and third steps can be considered as an indication of corrosion resistance behavior of concrete under acceleration test.

4. Conclusions

The presented study aimed at assessing the influence of nano-silica addition on the corrosion resistance of steel rebars embedded in UHPC. A new multi steps accelerated corrosion test was conducted, and the corrosion rate of steel rebars was determined at different time intervals. Based on the obtained results, the following conclusions are highlighted:

(1) The accelerated corrosion tests showed that the time to cracking in HPC is less than half the time in UHPC. In addition, UHPC-nS presented the best corrosion resistance performance, being time to cracking effectively increased with the nS addition.
(2) The use of nS in UHPC delays the initiation of corrosion in steel rebars, and thus it contributes to extending the service life of concrete structures. Results of Tafel and LPR tests indicate that the inclusion of nS effectively increases the polarization resistance of steel rebars in concrete. The higher polarization resistance of UHPC-nS, along with the lower corrosion current, indicates the enhancement of corrosion resistance of UHPC-nS.
(3) Corrosion rate measurements, based on LPR and Tafel techniques, point out that the UHPC specimens containing nS addition has the lowest corrosion rate (when compared with HPC and UHPC specimens).
(4) In general, results analysis of LPR tests indicate a similar corrosion behavior for all the three concrete mixtures, as compared with Tafel analysis; however, the LPR results show higher corrosion rate for the samples at similar testing condition and age.
(5) The accelerated corrosion test along with multi steps potentiodynamic polarization technique is an efficient test to assess the corrosion resistance of steel bar embedded in concrete specimens. Moreover, the corrosion potential itself cannot be considered as a reliable indicator of the real corrosion behavior of steel bars embedded in concrete specimens.

Acknowledgements

The authors thank the financial support of FCT, the Portuguese national funding agency for science, research and technology in the scope of the research project PTDC/ECM/098497/2008, entitled "Intelligent Super Skin. Enhanced Durability of Concrete Members".

References

[1] T. Ahlborn, Sustainability for the concrete bridge engineering community, ASPIRE (2008) 15–19.
[2] J.R. Mackechnie, M.G. Alexander, Using durability to enhance concrete sustainability, J. Green Build. 4 (3) (2009) 52–60.

[3] K. Kumar, Handbook on Repairs and Rehabilitation of RCC Buildings, Central Public Works Department (CPWD), New Delhi, 2002.
[4] Knudsen, A., Jensen, F.M., Klinghoffer, O., Skovsgaard, T. Cost-effective enhancement of durability of concrete structures by intelligent use of stainless steel reinforcement, in: Corrosion and Rehabilitation of Reinforced Concrete Structures, Florida, 1998.
[5] P. Virmani, J.M. Hooks, Corrosion Cost and Preventive Strategies in the United States, U.S. Federal Highway Administration, 2001.
[6] First International Symposium on Ultra High Performance Concrete, Kassel, Germany, 2004.
[7] Second International Symposium on Ultra High Performance Concrete, Kassel, Germany, 2008.
[8] The Third International Symposium on Ultra High Performance Concrete and Nanotechnology for High Performance Construction Materials, Kassel, Germany, 2012.
[9] B.A.B. Tayeh, B.H. Abu Johari, M.A. Megat Voo, Yen Lei, Utilization of ultra-high performance fibre concrete (UHPFC) for rehabilitation – a review, Procedia Eng. 54 (2013) 525–538.
[10] B.A. Tayeh, B.H. Abu Bakar, M.A. Megat Johari, Voo, Yen Lei, Mechanical and permeability properties of the interface between normal concrete substrate and ultra high performance fiber concrete overlay, Constr. Build. Mater. 36 (2012) 538–548.
[11] Brühwiler, E., Denarié, E. Rehabilitation of concrete structures using ultra-high performance fibre reinforced concrete, in: The Second International Symposium on Ultra High Performance Concrete, Kassel, Germany, 2008.
[12] Ghafari, E., Costa, H., Júlio, E., Portugal, A., Durães, L. Enhanced durability of ultra high performance concrete by incorporating supplementary cementitious materials, in: The Second International Conference Microdurability, Delft, Netherland, 2012.
[13] B.A. Tayeh, B.H. Abu Bakar, M.A. Johari, A.M. Zeyad, The role of silica fume in the adhesion of concrete restoration systems, Adv. Mater. Res. (2013).
[14] E. Ghafari, H. Costa, E. Júlio, A. Portugal, L. Durães, The effect of nanosilica addition on flowability, strength and transport properties of ultra high performance concrete, Mater. Des. 59 (2014) 1–9.
[15] Ghafari, E., Costa, H., Júlio, E., Portugal, A., Durães, L. Optimization of UHPC by adding nanomaterials, in: Proceedings of Third International Symposium on Ultra-high-performance Concrete and Nanotechnology for High Performance Construction Materials, Kassel, Germany, 2012.
[16] M.H. Beigi, J. Berenjian, O.L. Omran, A.S. Nik, I.M. Nikbin, An experimental survey on combined effects of fibers and nanosilica on the mechanical, rheological, and durability properties of self-compacting concrete, Mater. Des. 50 (2013) 1019–1029.
[17] M. Jalal, E. Mansouri, M. Sharifipour, A. Pouladkhan, Mechanical, rheological, durability and microstructural properties of high performance self-compacting concrete containing SiO_2 micro and nanoparticles, Mater. Des. 34 (2012) 389–400.
[18] X. He, X. Shi, Chloride permeability and microstructure of Portland cement mortars incorporating nanomaterials, J. Transp. Res. Board (2008) 13–21.
[19] H. Madani, A. Bagheri, T. Parhizkar, A. Raisghasemi, Chloride penetration and electrical resistivity of concretes containing nanosilica hydrosols with different specific surface areas, Cement Concr. Compos. 53 (2014) 18–24.
[20] M. Zhang, H. Li, Pore structure and chloride permeability of concrete containing nano-particles for pavement, Constr. Build. Mater. 25 (2) (2011) 608–616.
[21] A.M. Said, M.S. Zeidan, M.T. Bassuoni, Y. Tian, Properties of concrete incorporating nano-silica, Constr. Build. Mater. 36 (2012) 838–844.
[22] S. Abd El-Aleem, M. Heikal, W.M. Morsi, Hydration characteristic, thermal expansion and microstructure of cement containing nano-silica, Constr. Build. Mater. 59 (2014) 151–160.
[23] M. Heikal, S. Abd El-Aleem, W.M. Morsi, Characteristics of blended cements containing nano-silica, HBRC J. 9 (3) (2013) 243–255.
[24] E. Ghafari, H. Costa, E. Júlio, Statistical mixture design approach for eco-efficient UHPC, Cement Concr. Compos. 55 (2015) 17–25.
[25] Ghafari, E., Costa, H., Júlio, E. Development of ultra high performance self compacting concrete, in: Proceedings of the Fifth North American Conference on the SCC Design and Use of Self-Consolidating Concrete, Chicago, USA, 2013.
[26] E. Ghafari, C. Hugo, E. Júlio, RSM-based model to predict the performance of self-compacting UHPC reinforced with hybrid steel micro-fibers, Constr. Build. Mater. 66 (2014) 375–383.
[27] Ghafari, E., Bandarabadi, M., Costa, H., Júlio, E. Design of UHPC using Artificial Neural Networks, in: Tenth International Symposium on Brittle Matrix Composites, Warsaw, Poland, 2012.
[28] A.J. Al-Tayyib, M.M. Al Zahrani, Corrosion of steel reinforcement in polypropylene fiber reinforced concrete structure, ACI Mater. J. 87 (2) (1990) 108–113.
[29] M.M. Al-Zahrani, S.U. Al-Dulaijan, M. Ibrahim, H. Saricimen, F.M. Sharif, Effect of waterproofing coatings on steel reinforcement corrosion and physical properties of concrete, Cement Concr. Compos. 24 (1) (2002) 127–137.
[30] E. Güneyisi, T. Özturan, M. Gesoğlu, A study on reinforcement corrosion and related properties of plain and blended cement concretes under different curing conditions, Cement Concr. Compos. 27 (4) (2005) 449–461.
[31] E. Güneyisi, M. Gesoğlu, F. Karaboğa, K. Mermerdaş, Corrosion behavior of reinforcing steel embedded in chloride contaminated concretes with and without metakaolin, Compos. B Eng. 45 (1) (2013) 1288–1295.
[32] A.H. Al-Tayyib, M. Khan, Corrosion rate measurements of reinforcing steel in concrete by electrochemical techniques, ACI Mater. J. 85 (3) (1998) 172–177.
[33] J.A. Grubb, J. Blunt, C.P. Ostertag, T.M. Devine, Effect of steel microfibers on corrosion of steel reinforcing bars, Cem. Concr. Res. 37 (7) (2007) 1115–1126.
[34] A. Shamsad, Reinforcement corrosion in concrete structures, its monitoring and service life prediction – a review, Cement Concr. Compos. 25 (4–5) (2003) 459–471.
[35] M.A. El-Gelany, Short-term corrosion rate measurement of OPC and HPC reinforced concrete specimens by electrochemical techniques, Mater. Struct. 34 (7) (2001) 426–432.
[36] O.M. Bockris, A. Reddy, M. Gamboa-Aldeco, Modern electrochemistry 2a, fundamentals on electronics, Springer, New York, US, 2000.
[37] Dean, S.W.J. Electrochemical methods of corrosion testing, in: National Association of Corrosion Engineers, Houston, 1977.
[38] M. Ismail, M. Ohtsu, Corrosion rate of ordinary and high-performance concrete subjected to chloride attack by AC impedance spectroscopy, Constr. Build. Mater. 20 (7) (2006) 458–469.
[39] A. Poursaee, Potentiostatic transient technique, a simple approach to estimate the corrosion current density and Stern–Geary constant of reinforcing steel in concrete, Cem. Concr. Res. 40 (9) (2010) 1451–1458.
[40] P.R. Roberge (Ed.), Handbook of Corrosion Engineering, McGraw-Hill, New York, USA, 2000.
[41] M. Stern, A.L. Geary, A theoretical analysis of the slope of the polarization curves, Electrochem. Soc. 104 (1957) 56–63.
[42] T. Liu, R.W. Weyers, Modeling the dynamic corrosion process in chloride contaminated concrete structures, Cem. Concr. Res. 28 (3) (1998) 365–379.